Cellulose (2019) 26:6683–6700
https://doi.org/10.1007/s10570-019-02573-z

ORIGINAL RESEARCH

A hierarchical Ag_2O-nanoparticle/TiO_2-nanotube composite derived from natural cellulose substance with enhanced photocatalytic performance

Zehao Lin · Yongxin Lu · Jianguo Huang

Received: 25 March 2019 / Accepted: 17 June 2019 / Published online: 19 June 2019

Abstract A series of hierarchical Ag_2O-nanoparticle/TiO_2-nanotube heterostructured nanocomposites with varied Ag_2O contents were fabricated by employing natural cellulose substance as the template. The nanocomposites possessed fine three-dimensional porous network structures, which were composed of TiO_2 nanotubes and fine Ag_2O nanoparticles that anchored on the surfaces. The composites exhibited enhanced photocatalytic performances in degrading different organic pollutants under ultraviolet light irradiation. The optimal Ag_2O-NP/TiO_2-NT nanocomposites exhibited apparent rate constants of 0.62, 0.37 and 0.39 min^{-1} in photocatalytic degrading methylene blue, Rhodamine B and norfloxacin, respectively; which were correspondingly 2.6, 2.2, and 1.4 times higher than those of the pure TiO_2 nanotubes; and 3.9, 9.3, and 5.6 folds higher than those of the pure Ag_2O nanoparticles. It was demonstrated that the improved photocatalytic performances of the nanocomposites were attributed to the hierarchical nanotubular structures that inherited from the natural cellulose substances and the effective heterostructure between the titania and silver oxide phases derived from the unique structure. Hence, the close relationship between the cellulose derived structures and the photocatalytic performances of the nanocomposites were demonstrated. The related possible photocatalytic mechanism was revealed that the separation and transfer of the photogenerated electron–hole pairs was accelerated, and the superoxide radicals and reactive holes played a main role in the photocatalytic processes.

Electronic supplementary material The online version of this article (https://doi.org/10.1007/s10570-019-02573-z) contains supplementary material, which is available to authorized users.

Z. Lin · Y. Lu · J. Huang (✉)
Department of Chemistry, Zhejiang University, Hangzhou 310027, Zhejiang, China
e-mail: jghuang@zju.edu.cn

Graphic abstract

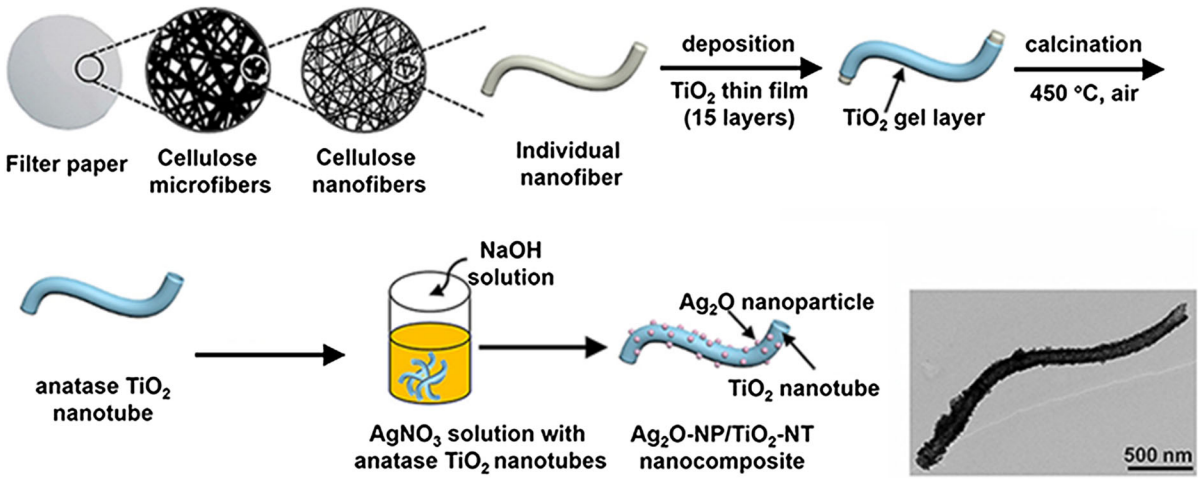

Keywords Cellulose · Biomimetic synthesis · Nanostructure · Self-assembly · Photocatalysis

Introduction

The rapid development of textile and paper industry has aroused severe pollution of various dyes, such as methylene blue, Rhodamine B, methyl orange and so on (Aboamera et al. 2018; Wang et al. 2018a, b; Min et al. 2019). It remains a challenge to treat these industrial waste water in a sustainable way. Since the water splitting by titania (TiO_2) electrode under ultraviolet (UV) light irradiation was discovered (Fujishima and Honda 1972), photocatalytic technology has attracted considerable attentions and been applied in the environmental issues widely (Ishimaki et al. 2018). Up to now, titania has been considered as the most remarkable semiconductor photocatalyst owing to its superior natures (Xu et al. 2018). However, the photocatalytic application in degrading dyes and other organic pollutants by titania is limited by the narrow light absorption, the high recombination rate of the photogenerated electron–hole pairs, and poor adsorption ability of the organic pollutants (Linsebigler et al. 1995). To solve these problems, a number of researches have been focused on designing heterojunctions between titania and other semiconductor substrates (Kansal et al. 2008; Li et al. 2009). Among these substrates, the p-type silver oxide semiconductor is deemed to be one of the most promising candidates because of its narrow band gap of 1.2 eV, facile preparation, and rather lower cost (Jiang et al. 2015). As reported, the formation of p-type-Ag_2O/n-type-TiO_2 heterojunction structure contributes to the formation of a built-in electric field within the space charge region and further facilitates the photocatalytic activity (Wei et al. 2016).

On the other hand, the morphology, particle size and dimensionality of the titania matters have significant impacts on the photocatalytic degradation processes. Since a Ag_2O/TiO_2 nanobelt structured composite was synthesized (Zhou et al. 2010), researchers have developed a number of Ag_2O/TiO_2 composites with different structures for the photocatalytic degradation of organic pollutants (Liu et al. 2015a, b). However, there still remains a challenge to develop a high-performance Ag_2O/TiO_2 composite photocatalyst with special structure, which could provide more active sites and larger specific surface area for the photocatalytic degradation of dyes and other organic pollutants with different molecular structures.

Bio-inspired synthesis could provide a solution to this issue by introducing the naturally formed, unique, complex, and hierarchical macro-to-nanoscale structural features of the natural biosubstances into artificial materials (Li et al. 2016). As a result, the structural advantages of the biomass substrates and the physicochemical properties of specific guest components are combined in a composite, which could not be

fabricated artificially by now (Li et al. 2018a; Jia and Li 2015). Cellulose substance is an ideal choice as the biomass substrate for bio-inspired materials syntheses due to its superior features of hierarchically three-dimensional cross-linked structure, environmental friendliness, and bio-compatibility (Kim et al. 2019; Su et al. 2017; Chen et al. 2018). The abundant surface hydroxyl groups of the cellulose fibers are convenient for the coating of specific guest components in the form of ultrathin films on the surfaces. Hence, the cellulose substance can be used as the templates or scaffolds for the fabrication of functional nanostructured materials. The unique structure and surface properties of the cellulose substance facilitate the fabrication of functional nanocomposites with hierarchical porous network structure.

In order to fabricate the well-designed functional composites, the layer-by-layer (LbL) self-assembly technique is regarded as one of the most effective and universal means (Zakaria et al. 2016; Ariga et al. 2013; Cai et al. 2015). This technique has been applied to the natural cellulose substances to give the nano-architectured porous materials, especially metal oxides by the template synthetic methods, which have displayed great potentials in the photocatalytic applications (Ariga et al. 2014; Fei and Li 2015). Therefore, it is significant to explore the potentials of the bio-inspired materials in the photocatalytic areas thoroughly. As reported by our previous works, titania-based nanocomposites derived from the natural cellulose substance showed good photocatalytic performances when employed as the photocatalysts, which is basically due to their unique hierarchical three-dimensional porous structures that inherited from the initial cellulose substance (Li and Huang 2016; Li et al. 2018b).

Although various kinds of cellulose templates have been applied to fabricate photocatalysts with improved performances, the photocatalytic activities of the cellulose derived nanocomposites were hindered owing to above-mentioned problems, and the formation of heterostructures on the cellulose derived matters was rarely reported (Mohamed et al. 2017, 2018; Xiao et al. 2018; Yoon et al. 2018). Can we fabricate specific titania based heterostructures uniformly and compactly to facilitate the separation of charges? Can the cellulose template derived structure promote the active sites and specific surface area of the nanocomposite? How do the cellulose template affect the photocatalytic performance of the nanocomposite? Can we find out the photocatalytic mechanism and the relationship between the structure and properties of the cellulose derived nanocomposite? Hence, we hypothesize that the hierarchical porous network structure of the cellulose substance is beneficial to the uniform formation of the heterostructures in-between titania and silver oxide, and further to the enhancement of photocatalytic performances of the nanocomposite obtained. In the present study, a novel Ag_2O-nanoparticle/TiO_2-nanotube (Ag_2O-NP/TiO_2-NT) heterostructured nanocomposite was fabricated by employing natural cellulose substance (commercial laboratory filter paper) as the template based on a LbL surface sol–gel process. It was composed of hierarchical TiO_2 nanotubes anchored with various amounts of Ag_2O nanoparticles on the surfaces. As being employed to the photocatalytic degradation of dyes and other organic pollutants, the composite exhibited excellent photocatalytic performance. The related possible explanations for the enhanced photocatalytic performance of the nanocomposites as well as the photocatalytic mechanism were clarified.

Materials and methods

Preparation of the hierarchical Ag_2O-NP/TiO_2-NT nanocomposites

The preparation process of the hierarchical Ag_2O-NP/TiO_2-NT nanocomposites is schematically illustrated in Scheme 1. According to our previous work (Luo and Huang 2015), the titania/cellulose composite was fabricated by a surface sol–gel method through depositing ultrathin titania gel films on each nanofiber of the quantitative ashless filter paper using titanium *n*-butoxide solution (100.0 mM in ethanol/toluene, v/v = 1:1) as the precursor and repeated for 15 times (Scheme 1a, b). The as-prepared titania/cellulose composite sheets were then calcined in air at 450 °C for 6 h to give the hierarchical anatase TiO_2 nanotubes (Scheme 1c).

Subsequently, the hierarchical Ag_2O-NP/TiO_2-NT nanocomposites with varied theoretical weight ratios of 1:1, 1:2, and 1:4 (Ag_2O:TiO_2) were synthesized by a simple precipitation method. For example, when the theoretical weight ratio was set as 1:1, 40.0 mg titania nanotubes powder was dispersed in 50.0 mL 6.80 mM

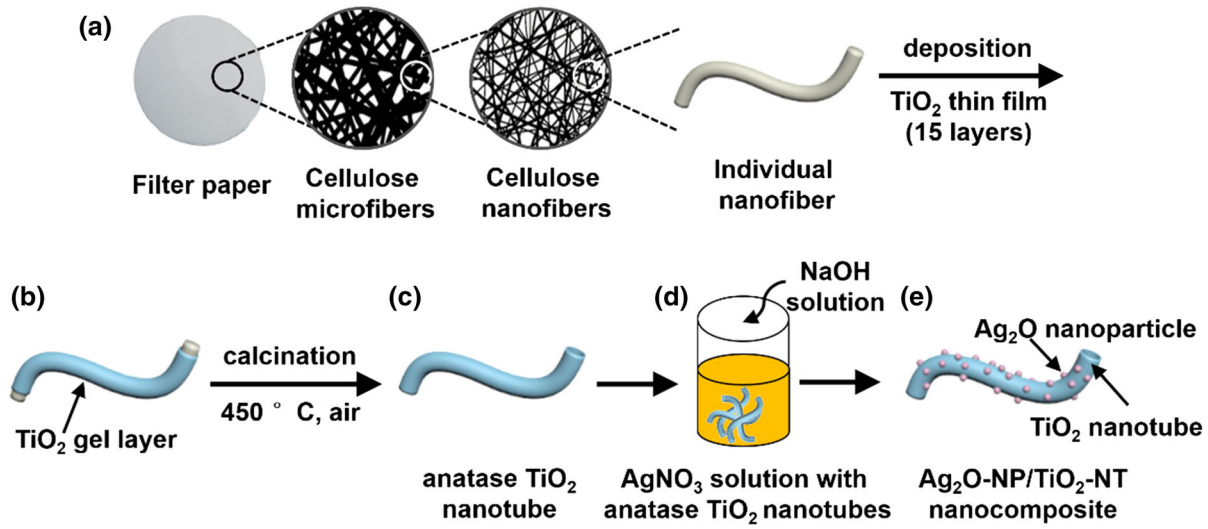

Scheme 1 Schematic illustration of the synthetic process of the hierarchical Ag_2O-NP/TiO_2-NT nanocomposites derived from natural cellulose substance. **a** The hierarchical structures of the original commercial laboratory filter paper, consisting of cellulose microfiber assemblies formed by nanofiber assemblies. **b** An individual nanofiber deposited with ultrathin TiO_2 gel layer. **c** An individual anatase TiO_2 nanotube. **d** The Ag_2O nanoparticles were coated on the TiO_2 nanotubes by a simple precipitation method. **e** An individual composite nanotube forming the final Ag_2O-NP/TiO_2-NT matter

$AgNO_3$ aqueous solution with stirring for 2 h, and then 20.0 mL 0.20 M NaOH aqueous solution was added dropwisely into the above suspension, followed by stirring for 1 h (Scheme 1d). Finally, the mixture obtained was centrifuged, and the obtained powder was collected and washed by deionized water and ethanol for several times, then dried at 37 °C in vacuum to give the hierarchical Ag_2O-NP/TiO_2-NT nanocomposites (Scheme 1e). The resultant nanocomposites with theoretical weight ratios of 1:1, 1:2, and 1:4 were confirmed to contain 51.8 wt%, 33.9 wt%, and 19.7 wt% contents of the Ag_2O component as demonstrated by the EDX analyses (Supplementary material, Fig. S1 and Table S1). Hence, the corresponding composites were denoted as 51.8%—Ag_2O-NP/TiO_2-NT, 33.9%—Ag_2O-NP/TiO_2-NT, and 19.7%—Ag_2O-NP/TiO_2-NT, respectively. Pure Ag_2O nanoparticles and pure TiO_2 nanotubes were prepared as the control materials (Supplementary material).

Photocatalytic tests

The photocatalytic degradation of methylene blue (MB), Rhodamine B (RhB) and norfloxacin (NFCX) was tested under the irradiation of UV light supplied by a high-pressure fluorescent mercury lamp (300 W, horizontal lamp-sample distance was 5.0 cm) by using a XPA-1 photoreactor (Nanjing Xujiang, China) with a constant temperature of 20 °C. Typically, 10.0 mg photocatalyst was added into 20.0 mL aqueous solution of the organic pollutant solution (10.0 mg/L), and was sonicated for 1 min to form a homogeneous suspension, followed by stirring in dark for 30 min to achieve an adsorption–desorption equilibrium of the model pollutant. During the irradiation process, 5.0 mL of the suspension was taken away at different time intervals, and centrifuged at 12,000 rpm for 3 min, followed by being analyzed on a Shimadzu UV-2450 spectrophotometer, and then recycled. Besides, the evaluation methods of the photocatalytic stability and mechanisms of the nanocomposite were described in Supplementary material.

Results and discussion

Structural characterizations of the Ag_2O-NP/TiO_2-NT nanocomposites

The fabrication process of the hierarchical Ag_2O-NP/TiO_2-NT nanocomposites derived from natural cellulose substance is schematically illustrated in Scheme 1. The ultrathin titania gel layers were coated

on each cellulose nanofiber of the filter paper by the LbL surface sol–gel process and calcined to give the anatase TiO_2 nanotubes (Scheme 1a–c). After that, the nanocomposites were obtained through a simple precipitation method (Scheme 1d, e).

The powder X-ray diffraction (XRD) patterns of all samples are shown in Fig. 1. All spectra of the Ag_2O-NP/TiO_2-NT nanocomposites show the diffraction peaks located at 2θ = 25.3°, 37.8°, 48.0°, 53.9°, 55.1°, and 62.7°, which are ascribed to the (101), (004), (200), (105), (211), and (204) planes of anatase phase titania (JCPDS No. 21-1272) (Liu et al. 2015b). In addition, the spectrum of the 51.8%—Ag_2O-NP/TiO_2-NT sample displays another four diffraction peaks located at 2θ = 32.8°, 38.1°, 54.9°, and 65.4°, which are indexed to the (111), (200), (220), and (311) planes of cubic phase silver oxide (JCPDS No. 41-1104) (Chu et al. 2016). With the decrease in the Ag_2O contents, the peak intensities of cubic phase silver oxide become weaker, and finally vanish in the spectrum of the 19.7%—Ag_2O-NP/TiO_2-NT sample. For the spectrum of the 33.9%—Ag_2O-NP/TiO_2-NT sample, the ambiguous diffraction peaks located at 2θ = 38.0° and 55.0° are indexed to the (004) and (211) planes of anatase phase titania, or (200) and (220) planes of cubic phase silver oxide due to the nearby positions in the XRD patterns of them. As compared with the pure Ag_2O nanoparticles and TiO_2 nanotubes, all Ag_2O-NP/TiO_2-NT nanocomposites exhibit only characteristic peaks of both Ag_2O and TiO_2 components, confirming the high purity of these nanocomposites.

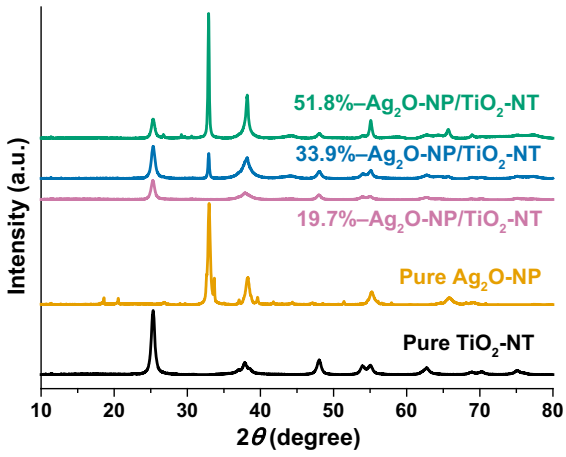

Fig. 1 XRD patterns of the cellulose-derived hierarchical Ag_2O-NP/TiO_2-NT nanocomposites with varied Ag_2O contents, and the spectra of the pure Ag_2O nanoparticles and TiO_2 nanotubes

Figure 2 shows the structures and morphologies of the 19.7%—Ag_2O-NP/TiO_2-NT nanocomposite as observed by electron microscopes. The field emission scanning electron microscope (FE-SEM) micrograph (Fig. 2a) reveals that the nanocomposite is composed of microfiber assemblies, and each microfiber is formed by nanofibers by nanofiber assemblies, which retains the fine network structures of the initial cellulose substance. In more details, the enlarged FE-SEM image (Fig. 2b) shows that Ag_2O nanoparticles are distributed uniformly and densely on the surfaces of the TiO_2 nanotubes. In comparison with the pure TiO_2 nanotubes and Ag_2O-NP/TiO_2-NT nanocomposites (Supplementary material, Fig. S2a, c and e), the hierarchical nanotubular structures are not affected by the coating of the Ag_2O nanoparticles. Besides, the pure Ag_2O nanoparticles are hundreds of nanometers in size and formed by aggregated fine nanoparticles (Supplementary material, Fig. S3). The transmission electron microscope (TEM) images of an individual nanocomposite tube clearly display that Ag_2O nanoparticles with a fine size (ca. 9.4 nm) and a narrow size distribution (± 2.6 nm) (Supplementary material, Fig. S4) are anchored uniformly on the surface of the titania nanotube with a tube width of ca. 130 nm that is formed by titania nanoparticles compactly with a thickness of ca. 7.5 nm (Fig. 2c, d). With the increment in the Ag_2O contents of the Ag_2O-NP/TiO_2-NT nanocomposites, the TiO_2 nanotubes are covered with more Ag_2O nanoparticles (Supplementary material Fig. S2b, d and f). The high resolution transmission electron microscope (HR-TEM) micrograph (Fig. 2e) exhibits two kinds of lattice spacings of 0.354 and 0.235 nm, which match well with those of the (101) plane of anatase phase titania and the (200) plane of cubic phase silver oxide (Kaur et al. 2017), respectively. The selected area electron diffraction (SAED) pattern (Fig. 2f) presents tanglesome diffraction rings, which are typical of anatase phase titania and cubic phase silver oxide, and the Nos. 1–5 diffraction rings are mainly attributed to the (101), (112), (200), (211), and (215) reflections of anatase phase titania (Luo et al. 2014; Mandari et al. 2017). However, due to the similar lattice spacings, the diffraction rings of Nos. 2–4 are also assigned to the

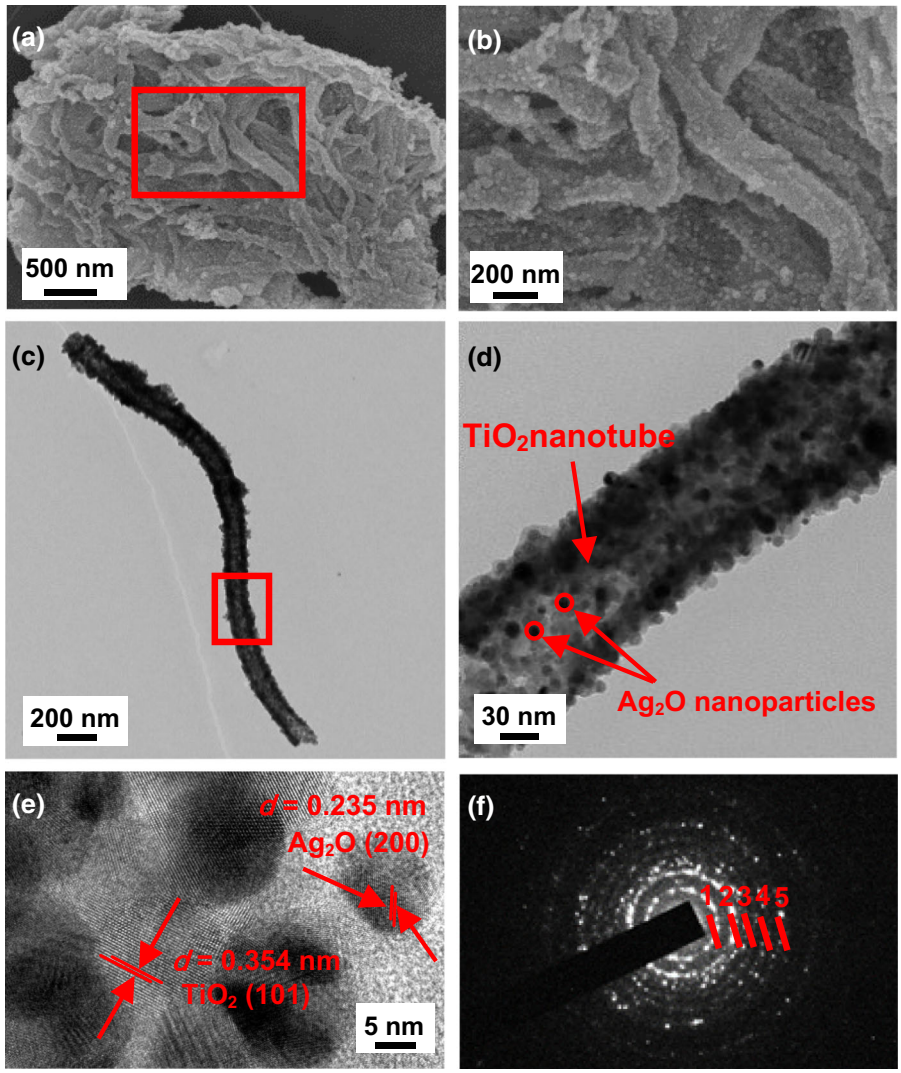

Fig. 2 Electron micrographs of the cellulose-derived hierarchical 19.7%—Ag_2O-NP/TiO_2-NT nanocomposite. **a**, **b** Low and high magnification FE-SEM images of the nanocomposite showing the nanotube assemblies, the red box in (**a**) indicates the enlarged area as shown in (**b**). **c** TEM image of an individual nanotube of the nanocomposite. **d** TEM image of the enlarged area boxed in (**c**). **e** HR-TEM image of the nanocomposite tube surface, demonstrating the existence of lattice planes of Ag_2O and TiO_2 components. **f** SAED pattern of the sample. (Color figure online)

(200), (211), and (220) reflections of cubic phase silver oxide (Wei et al. 2011), respectively.

The energy dispersive X-ray spectrometry (EDX) element mapping images of the 19.7%—Ag_2O-NP/TiO_2-NT nanocomposite tube (Fig. 3) reveal that the rounded Ag_2O nanoparticles (red points) are anchored on the compact nanotube surface made up of TiO_2 (green points) uniformly. Moreover, some of the signals of the titanium and silver elements are interlaced, indicating the existence of the Ag_2O-NP/TiO_2-NT heterostructure. All the results of the morphological characterization reveal that the Ag_2O-NP/TiO_2-NT nanocomposite inherits the hierarchical porous network structure of the initial natural cellulose substance, uniform heterostructure in-between the Ag_2O nanoparticle and the titania nanotube was achieved.

As shown in Fig. 4, the surface chemical composition and chemical states of Ag, Ti and O elements of the 51.8%—Ag_2O-NP/TiO_2-NT nanocomposite were characterized by X-ray photoelectron spectroscopy (XPS) measurement. The XPS survey spectrum (Fig. 4a) suggests that the nanocomposite is only composed of the Ag, Ti, and O elements. The high-resolution spectrum of the Ag(3*d*) region (Fig. 4b) exhibits the spin–orbit split lines of Ag($3d_{5/2}$), and Ag($3d_{3/2}$) at 367.7, and 373.7 eV, respectively; which indicates that the Ag element exists in one valence state (Ag(I)) of Ag_2O (Sarkar et al. 2013). The high-resolution spectrum of the Ti(2*p*) region (Fig. 4c)

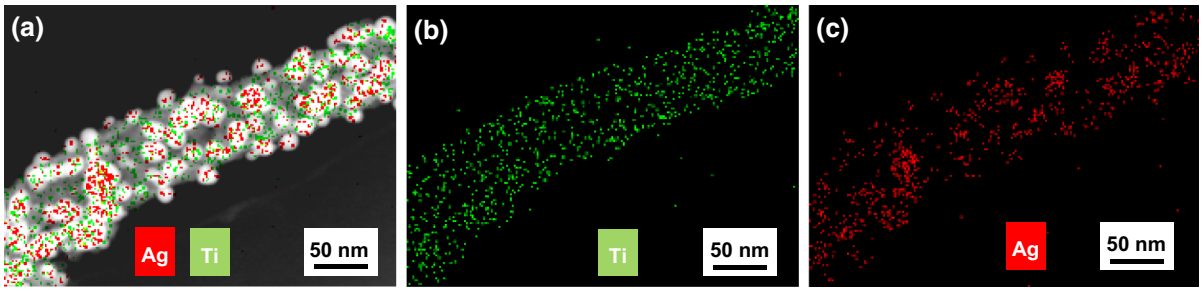

Fig. 3 EDX element mapping of the titania and silver elements of an individual nanotube in the 19.7%—Ag_2O-NP/TiO_2-NT nanocomposite sample derived from natural cellulose substance

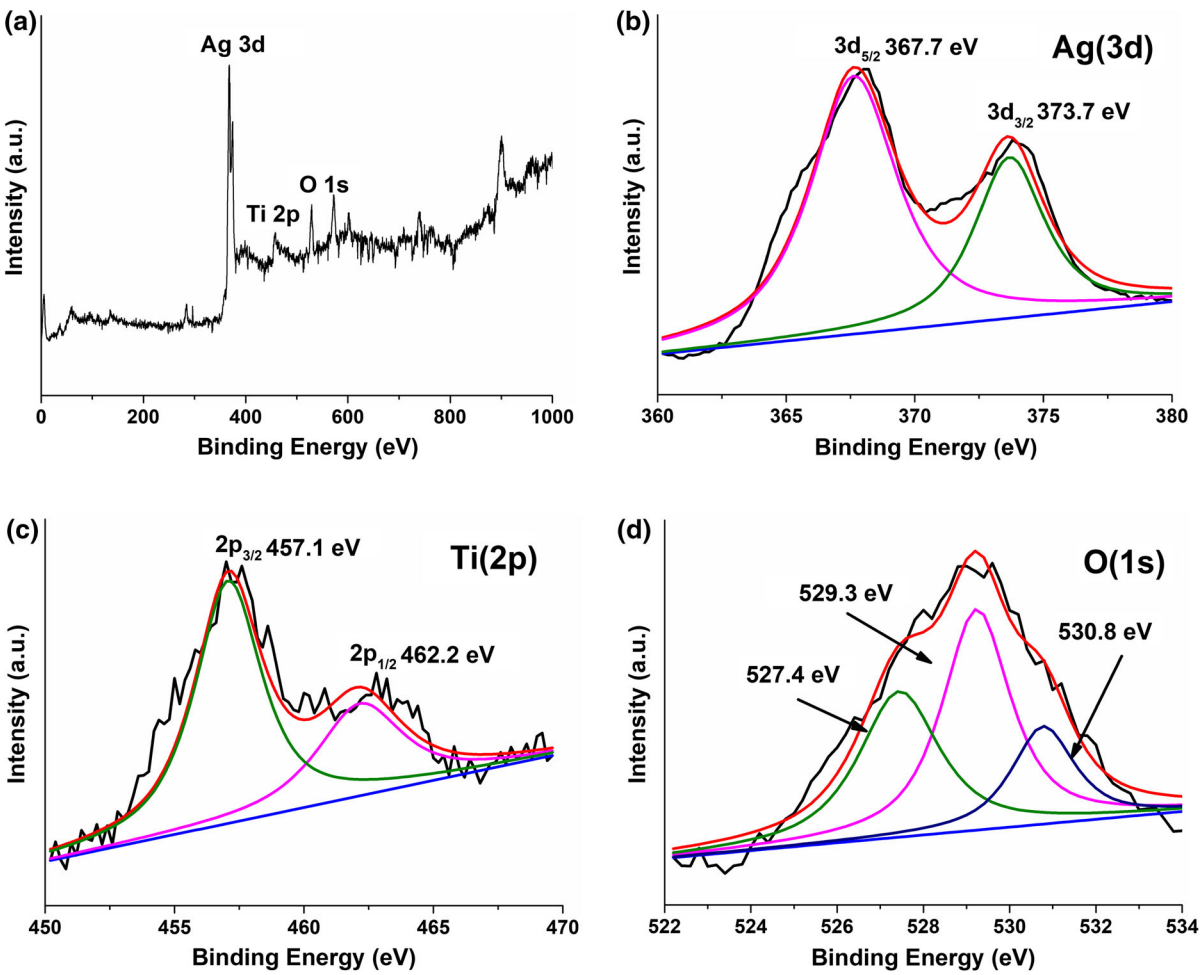

Fig. 4 XPS spectra of the cellulose-derived hierarchical 51.8%—Ag_2O-NP/TiO_2-NT nanocomposite. **a** XPS survey spectrum of the nanocomposite. **b–d** High-resolution spectra of the Ag(3*d*), Ti(2*p*), and O(1*s*) regions of the nanocomposite, respectively

exhibits two peaks at 457.1, and 462.2 eV, which are attributed to the typical binding energies for Ti($2p_{2/3}$) and Ti($2p_{1/2}$) of TiO_2 (Liu et al. 2017), respectively. Besides, the energy gap between the two peaks is 5.1 eV, which agrees well with the typical energy gap of the four valence state of Ti element in titania (Gu and Huang 2013). The high-resolution spectrum of the O(1*s*) region (Fig. 4d) shows three peaks at 527.4,

529.3, and 530.8 eV, which correspond to the oxygen lattices in TiO_2 (Hu et al. 2017), the oxygen lattices in Ag_2O (Hao et al. 2018), and the external −OH group or the H_2O molecules absorbed on the surface of the sample (Yu et al. 2015). As a comparison, the Ag_2O/TiO_2 composite was prepared with the same condition as the 51.8%—Ag_2O-NP/TiO_2-NT nanocomposite but without using of the cellulose template. The high-resolution XPS spectrum of the Ti(2*p*) region of the Ag_2O/TiO_2 composite (Supplementary material, Fig. S5) exhibits the similar peaks at 458.0 and 463.7 eV, which are attributed to the Ti element of TiO_2. In comparison with the peaks at 458.5 and 464.2 eV in the high-resolution XPS spectrum of the Ti(2*p*) region of the pure TiO_2 (Gu and Huang 2013), the shifts of the corresponding peaks in the spectrum of the 51.8%—Ag_2O-NP/TiO_2-NT nanocomposite are more obvious than those in the spectrum of the Ag_2O/TiO_2 composite, indicating the more efficient and uniform formation of the Ag_2O/TiO_2 heterostructure in the 51.8%—Ag_2O-NP/TiO_2-NT nanocomposite due to the significant effects of the cellulose template.

The nitrogen adsorption–desorption isotherms (Fig. S5a, c, and e) of Ag_2O-NP/TiO_2-NT nanocomposites all exhibit type IV adsorption isotherms with H3-type hysteresis loops according to the IUPAC classification, confirming the mesoporous structure of the nanocomposites (Gao et al. 2017). The values of the Brunauer–Emmett–Teller (BET) specific surface area (S_{BET}) (Supplementary material, Table S2) of the nanocomposites decrease as the increased proportion of the Ag_2O components, indicating that the porosity decreases in accordance with the enhanced amounts of the anchored Ag_2O nanoparticles. Besides, all of them are higher than that of the pure TiO_2 nanotubes (26.4 m^2/g) (Liu et al. 2010), which is helpful to the adsorption of the organic pollutants. All the Barrett–Joyner–Halenda (BJH) pore size distribution curves (Fig. 5b, d, f) of the nanocomposites exhibit one peak at below 10 nm that assigned to the network structure and voids in-between confined TiO_2 nanoparticles, and the other one at about 50 nm is probably caused by the gaps in-between the anchored Ag_2O nanoparticles. Moreover, the 51.8%—Ag_2O-NP/TiO_2-NT nanocomposite owns the largest pore size, which is ascribed to the larger gaps in-between the Ag_2O nanoparticles than those in-between the TiO_2 nanoparticles. The 33.9%—Ag_2O-NP/TiO_2-NT nanocomposite displays lower pore size than that of the 19.7%—Ag_2O-NP/TiO_2-NT nanocomposite, demonstrating that the Ag_2O nanoparticles on the surface of the TiO_2 nanotubes block the pores between the TiO_2 nanoparticles, while new pores between Ag_2O nanoparticles are not formed because the size of Ag_2O nanoparticles is larger than that of the TiO_2 nanoparticles. The BJH pore size distribution curve of the Ag_2O/TiO_2 composite prepared without using of the cellulose template (Supplementary material, Fig S6) shows only a peak at about 30 nm without the peak below 10 nm, which is mainly attributed to the gaps in-between the aggregated Ag_2O particles, revealing that the TiO_2 phase of the Ag_2O/TiO_2 composite is not porous and it cannot inhibit the aggregation of Ag_2O particles. It has been demonstrated that the hierarchical porous network structure of the cellulose template provides the Ag_2O-NP/TiO_2-NT nanocomposite with superior porous properties and the uniform formation of Ag_2O nanoparticles of the nanocomposite. The different properties of pores in the nanocomposites result in the differences in the adsorption capacities towards different organic pollutants.

According to the above results, the formation mechanism of the Ag_2O-NP/TiO_2-NT nanocomposite is discussed as follows. In the sol–gel process, the titanium *n*-butoxide molecules are chemically adsorbed with the abundant surface hydroxyl groups of the cellulose fibers via covalent bond, while the physically absorbed molecules are washed off. Afterwards, the chemically absorbed titanium *n*-butoxide molecules are turned into the ultrathin titania gel layer by hydrolysis, which provides abundant hydroxyl groups for the subsequent deposition of titania layers to give the titania/cellulose composite. Due to the three-dimensional network structure of the cellulose template, the aggregation of TiO_2 nanoparticles is inhibited when the titania/cellulose composite is calcined in air, and the obtained TiO_2 nanotubes inherit the unique structure of the cellulose template and display porous structure. When the TiO_2 nanotubes are mixed with $AgNO_3$ solution, Ag^+ is dispersed on the tube surfaces uniformly and compactly because of the unique hierarchical network structure of the TiO_2 nanotubes, and then the precipitation reaction takes place by Eq. (1) to generate the Ag_2O-NP/TiO_2-NT nanocomposite. The aggregation of the fine Ag_2O nanoparticles is controlled benefited from the hierarchical porous network structure of the TiO_2 nanotubes.

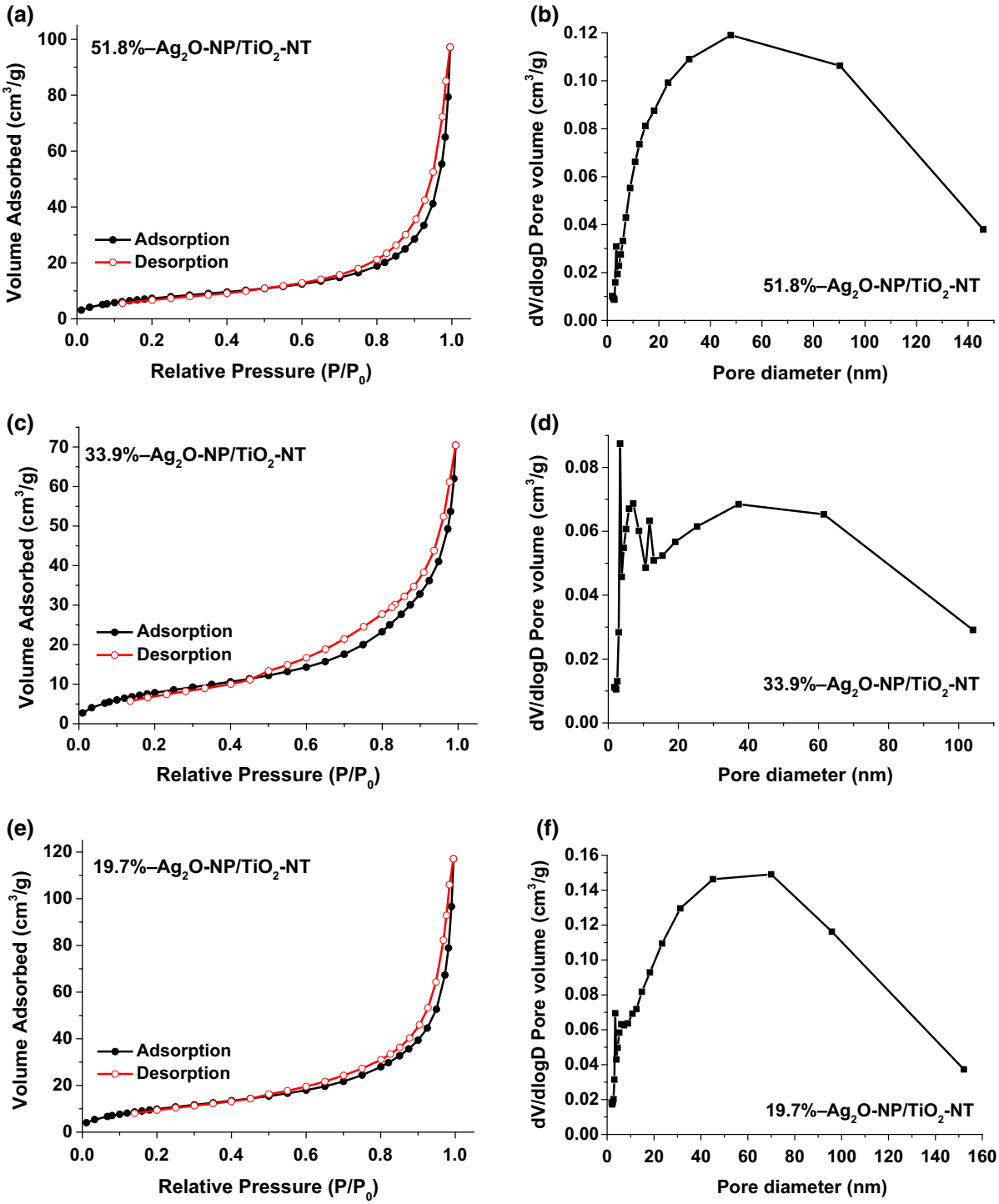

Fig. 5 Nitrogen adsorption–desorption isotherms and the corresponding pore size distribution curves analyzed from the adsorption branch of the isotherms of the cellulose-derived hierarchical 51.8%—Ag_2O-NP/TiO_2-NT (**a**, **b**), 33.9%—Ag_2O-NP/TiO_2-NT (**c**, **d**) and 19.7%—Ag_2O-NP/TiO_2-NT (**e**, **f**) nanocomposites

$$2Ag^{+} + 2OH^{-} \rightarrow 2AgOH \rightarrow Ag_2O + H_2O \quad (1)$$

Optical properties of the hierarchical Ag_2O-NP/TiO_2-NT nanocomposites

As shown in Fig. 6a, the UV/Vis diffuse reflectance spectra (DRS) of the Ag_2O-NP/TiO_2-NT nanocomposites all exhibit two absorption bands centered at 410 and 270 nm, which are assigned to the visible and UV light absorption (Lalitha et al. 2010). The pure TiO_2 nanotube sample only exhibits a narrow UV light absorption band centered at 260 nm, while the pure Ag_2O nanoparticle sample shows another broad visible light absorption band centered at 410 nm. In addition, the estimated band gaps (E_g) of the Ag_2O-NP/TiO_2-NT nanocomposites (Fig. 6b and Table S2) are in the range of 2.08–2.67 eV, and those of the pure TiO_2 nanotubes and Ag_2O nanoparticles are 3.04 eV and 1.46 eV, respectively; which are in good agreement with the reported data (Zelekew et al. 2017; Kumar et al. 2016). In comparison with the pure TiO_2 nanotubes, the decrease in E_g of the nanocomposites is basically due to the aligned Fermi levels of the *p*-type Ag_2O and *n*-type TiO_2, together with new band structures, which is attributed to the efficient formation of the heterostructures (Liu et al. 2019). It results in the significantly enhanced UV and visible light responses and promoted photoexcitation efficiency. Besides, the sequence of band gaps of the Ag_2O-NP/TiO_2-NT nanocomposites follows as 19.7%—Ag_2O-NP/TiO_2-NT (2.08 eV) > 51.8%—Ag_2O-NP/TiO_2-NT (2.34 eV) > 33.9%—Ag_2O-NP/TiO_2-NT

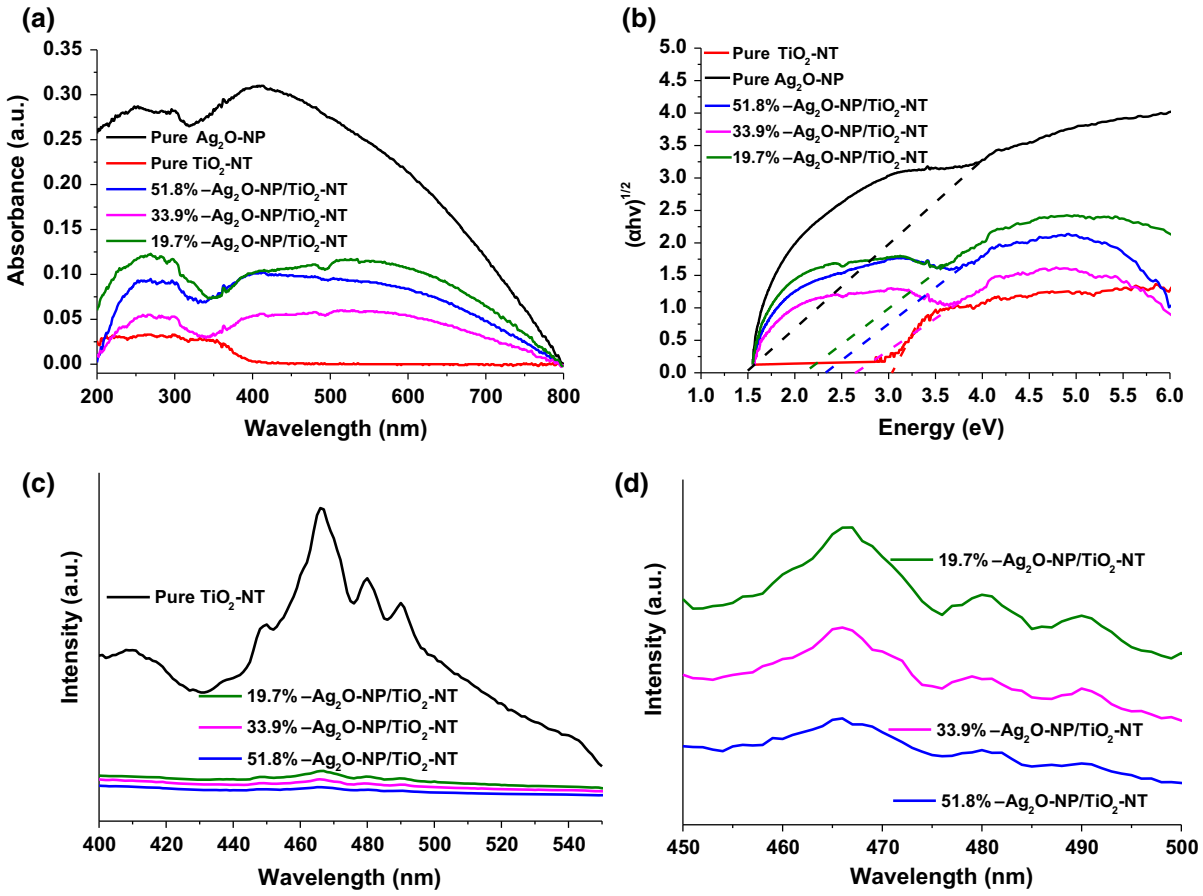

Fig. 6 Optical spectra of the cellulose-derived hierarchical Ag_2O-NP/TiO_2-NT nanocomposites with varied Ag_2O contents, the pure Ag_2O nanoparticles and TiO_2 nanotubes. **a** UV/Vis DRS spectra. **b** The corresponding Tauc plot considering the indirect energy gap nature and respective energy gaps estimated by the intercept on the *x*-axis. **c** PL spectra under a laser excitation of 350 nm. **d** The enlarged PL spectra of the Ag_2O-NP/TiO_2-NT nanocomposites in the 450–500 nm region of (**c**)

(2.67 eV), as shown in Table S2 (Supplementary material). The lowest band gap of the 19.7%—Ag_2O-NP/TiO_2-NT with the lowest content of Ag_2O is attributed to the largest band bending due to the most effective formation of the heterostructures (Paul et al. 2016). With the increase of the Ag_2O content, the light penetration into the heterostructures is hindered partly, leading to the larger band gap of the 33.9%—Ag_2O-NP/TiO_2-NT nanocomposite (Sarkar et al. 2013). However, when the Ag_2O content is further increased, Ag_2O nanoparticles covered the surfaces of the TiO_2 nanotubes fully in the 51.8%—Ag_2O-NP/TiO_2-NT nanocomposite, leading to the lower band gap due to the rather low band gap of the pure Ag_2O nanoparticles.

The photoluminescence (PL) spectra (Fig. 6c) of the Ag_2O-NP/TiO_2-NT nanocomposites and pure TiO_2 nanotubes all exhibit one strong emission peak located at 467 nm that is attributed to the recombination of photogenerated electron–hole pairs (Chu et al. 2016), and other weaker ones located at 450, 480 and 490 nm that are assigned to the free recombination of exciton centers, the surface defects, and the oxygen vacancies of the samples, respectively (Chu et al. 2016; Kaur et al. 2017). It is obvious that the nanocomposites exhibit rather lower PL emission intensity than the pure TiO_2 nanotubes, indicating that the recombination of the photogenerated electrons and holes is effectively suppressed in the nanocomposites. Besides, the intensity of the PL emission weakens slightly with the increase in the contents of Ag_2O of the nanocomposites (Fig. 6d), which is attributed to the higher separation and transfer efficiency of the photogenerated electron–hole pairs due to the enhanced amount of the heterostructures. The increased photoexcitation efficiency and faster migration efficiency of the photogenerated electron–hole pairs in the Ag_2O-NP/TiO_2-NT nanocomposites are due to the uniform and stable formation of the heterostructures derived from the unique structure of the natural cellulose substance, which would effectively enhance the photocatalytic performances of the nanocomposite.

Photocatalytic performance of the Ag_2O-NP/TiO_2-NT nanocomposites

To evaluate the photocatalytic performances of the Ag_2O-NP/TiO_2-NT nanocomposites, MB, RhB and NFCX are selected as the organic contaminants and degraded under UV light irradiation using the nanocomposites as the photocatalysts. The degradation profiles and the corresponding pseudo-first-order simulation results are displayed in Fig. 7. In order to obtain the intuitive photocatalytic reactivity quantitatively, corresponding values of the adsorption capacity (q_e) towards the organic contaminants, apparent rate constant (K_{app}) determined by the pseudo-first-order kinetic equation, and real photocatalytic efficiency over unit area (K_s) of the Ag_2O-NP/TiO_2-NT nanocomposites are listed in Table S3 (Supplementary material), respectively. Herein, values of q_e, K_{app} and K_s are calculated by the following equations (Wang et al. 2018a):

$$q_e = (C_i - C_0)V/(mS_{BET}) \quad (2)$$

$$ln(C_0/C) = K_{app}t \quad (3)$$

$$K_s = K_{app}/S_{BET} \quad (4)$$

where C_i, C_0, and C are the initial concentration (10.0 mg/L), equilibrium concentration, and concentration after certain irradiation time (t in min) of the organic contaminants solution, respectively; V is the volume (in L) of the solution, and m is the mass (in g) of the photocatalyst.

Before the photocatalytic degradation tests, the adsorption–desorption equilibrium was achieved and the q_e of the Ag_2O-NP/TiO_2-NT nanocomposites on the three targeted pollutants follows the same order: 51.8%—Ag_2O-NP/TiO_2-NT > 33.9%—Ag_2O-NP/TiO_2-NT > 19.7%—Ag_2O-NP/TiO_2-NT, which exhibits the inverse order of the values of S_{BET}, indicating that the adsorption capacities of the Ag_2O-NP/TiO_2-NT nanocomposites show more association with the pore size than the specific surface area. Besides, the adsorption capacities of the nanocomposites are considerably higher than those of the pure TiO_2 nanotubes or Ag_2O nanoparticles, which is attributed to the unique hierarchical porous network structure of it derived from the cellulose substance, the uniform formation of the heterostructures, as well as the higher specific surface area. However, all the nanocomposites exhibit higher adsorption capacities towards MB and NFCX than RhB, which could be speculated that the MB and NFCX molecules contain weakly negatively charged N atoms that play a role as an electron donating group and could be liable to inject electrons

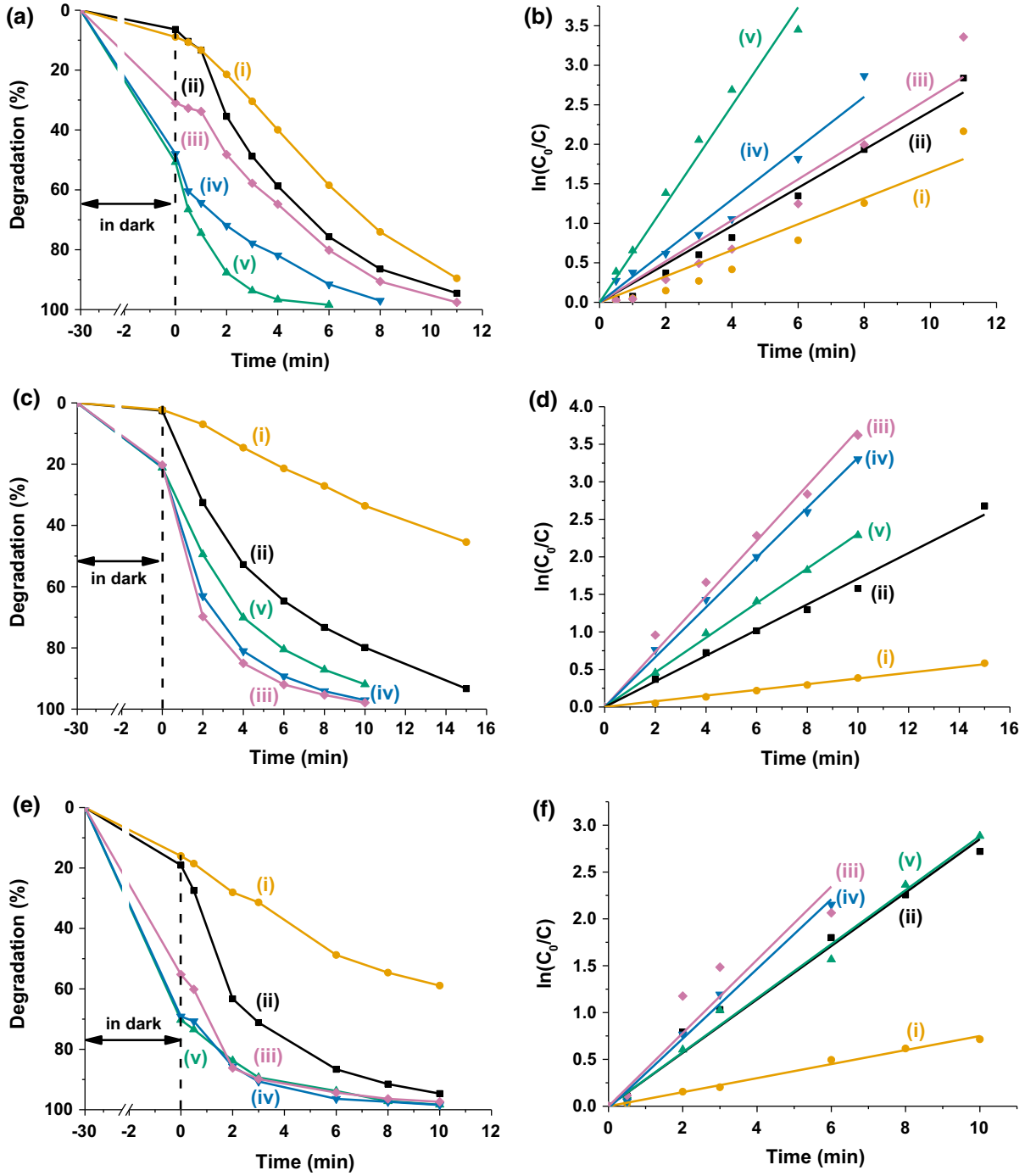

Fig. 7 The photocatalytic degradation profiles and the corresponding pseudo-first-order simulations of the pure Ag_2O nanoparticles (i), the pure TiO_2 nanotubes (ii), and the cellulose-derived hierarchical 19.7%—Ag_2O-NP/TiO_2-NT nanocomposites (iii), 33.9%—Ag_2O-NP/TiO_2-NT nanocomposites (iv), and 51.8%—Ag_2O-NP/TiO_2-NT nanocomposites (v) in degrading **a**, **b** MB, **c**, **d** RhB, and **e**, **f** NFCX under UV light irradiation

to empty d orbit of the metal elements, while the O atoms of the RhB molecules do not play the same role (Wang et al. 2018a). The outstanding adsorption capacities of the nanocomposites provide a prerequisite for the excellent photocatalytic degradation performance.

After the adsorption equilibrium of the model pollutant was achieved, the photocatalytic degradation tests were initiated and the calculated K_{app} and corresponding goodness of fit (R^2) of the samples in degrading organic pollutants are shown in Table S4 (Supplementary material). It is seen that all of the photocatalytic degradation reactions are well consistent with the pseudo-first-order due to the high values of R^2. As shown in Fig. 7a, b, the optimal sample in degrading MB is 51.8%—Ag_2O-NP/TiO_2-NT and achieves a degradation rate of 99% after irradiation for 6 min. The K_{app} of it (0.62 min^{-1}) exhibits 2.6 and 3.9 folds higher than that of the pure TiO_2 nanotubes (0.24 min^{-1}) and Ag_2O nanoparticles (0.16 min^{-1}), respectively. Figure 7c, d reveal that the optimum sample in degrading RhB is 19.7%—Ag_2O-NP/TiO_2-NT and it degrades 98% RhB after irradiation for 10 min. The K_{app} of it (0.37 min^{-1}) is 2.2 and 9.3 times higher than that of the pure TiO_2 nanotubes (0.17 min^{-1}) and Ag_2O nanoparticles (0.04 min^{-1}), respectively. The colorless organic pollutant NFCX is photocatalytic degraded to eliminate the indirect dye photosensitization as shown in Fig. 7e, f. It is seen that the 19.7%—Ag_2O-NP/TiO_2-NT nanocomposite displays the superior photocatalytic performance with a removal rate of 98% after 8 min irradiation, and the K_{app} of it (0.39 min^{-1}) shows 1.4 and 5.6-fold increment as compared with that of the pure TiO_2 nanotubes (0.28 min^{-1}) and Ag_2O nanoparticles (0.07 min^{-1}), respectively. As expected, all Ag_2O-NP/TiO_2-NT nanocomposites show enhanced photocatalytic performances in degrading different organic pollutants as compared with the pure TiO_2 nanotubes and Ag_2O nanoparticles, which is ascribed to the increased adsorption capacities and the enhanced amount and lower recombination rate of the photogenerated electron–hole pairs. It demonstrates that the uniform and efficient formation of the heterostructures derived from the three-dimensional porous network structures of the nanocomposites result in the above improvements, which is benefited from the cellulose template structure. It also reveals the obvious relationship in-between the unique structure of the Ag_2O-NP/TiO_2-NT nanocomposites that derived from the cellulose substance and their corresponding photocatalytic degradation performances.

To further analyze the difference of the photocatalytic performances of the Ag_2O-NP/TiO_2-NT nanocomposites towards different organic pollutants, the sequences of K_{app} and K_s of the nanocomposites are summarized. (Supplementary material, Table S5). The order of K_s in degrading MB is identical to that of K_{app}. However, the K_s in degrading RhB and NFCX displays the same sequence but opposite to that of MB, where the orders of the 33.9%—Ag_2O-NP/TiO_2-NT and 19.7%—Ag_2O-NP/TiO_2-NT nanocomposites are interchangeable when K_{app} is considered, revealing that the higher specific surface area of the 19.7%—Ag_2O-NP/TiO_2-NT nanocomposite results in more active sites in the photodegradation process of RhB and NFCX. Besides, the differences in optimal samples also demonstrates that the prominent advantages in MB adsorption capacity and separation efficiencies of the photogenerated electrons and pairs of the 51.8%—Ag_2O-NP/TiO_2-NT nanocomposite greatly promotes its photocatalytic performance. However, the superior photocatalytic performances in degrading RhB and NFCX of the 33.9%—Ag_2O-NP/TiO_2-NT and 19.7%—Ag_2O-NP/TiO_2-NT nanocomposites are attributed to the more active sites and fewer amount of Ag_2O nanoparticles due to the poorer photocatalytic performance of the pure Ag_2O nanoparticles.

In comparison with other Ag_2O/TiO_2 composite photocatalysts reported in the literatures (Supplementary material, Table S6), the cellulose-derived hierarchical Ag_2O-NP/TiO_2-NT heterostructured nanocomposites exhibit much superior photocatalytic performances under UV light irradiation than some of the reported Ag_2O/TiO_2 composites. The excellent photocatalytic performance of the current nanocomposite is mainly attributed to the combination of the hierarchical porous network structure and the uniform formation of the heterostructures due to the natural cellulose substance template, as illustrated above.

The photocatalytic stability determines the practical application potentials of the photocatalysts. The degradation efficiencies (Fig. 8a) of 51.8%—Ag_2O-NP/TiO_2-NT nanocomposite towards MB are 99%, 89% and 72% for the three cycles, respectively. It reveals that the photocatalytic performance of the nanocomposite maintains a high stability, which is attributed to its hierarchical porous network structure

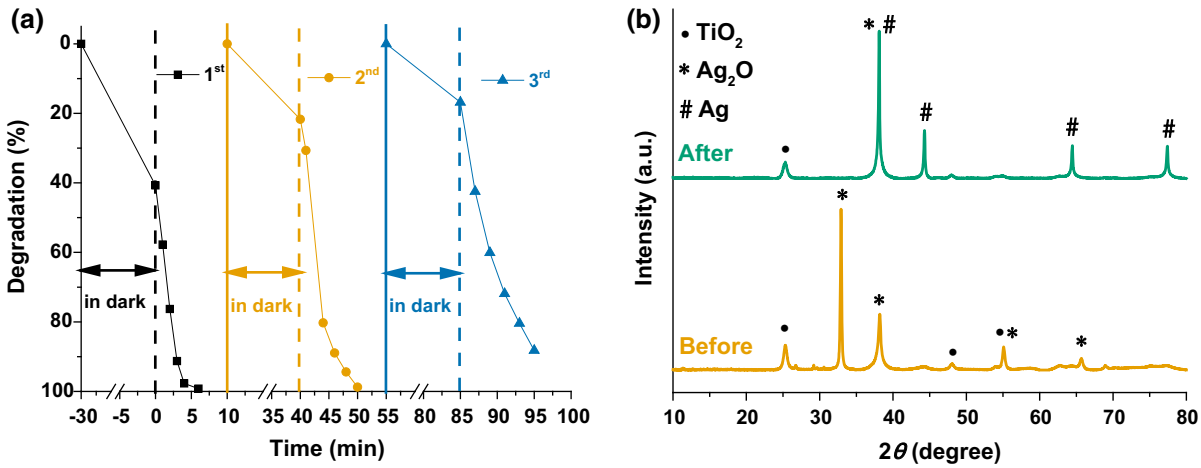

Fig. 8 Photocatalytic stability tests of the cellulose-derived hierarchical 51.8%—Ag_2O-NP/TiO_2-NT nanocomposites. **a** The photocatalytic degradation profiles of MB for three cycles by the nanocomposite under UV light irradiation. **b** XRD patterns of the nanocomposite before and after the cycling experiments

derived from the cellulose substance. The XRD patterns (Fig. 8b) exhibit that the characteristic peak located at $2\theta = 32.8°$ that indexed to the (111) plane of cubic phase silver oxide disappears after the photocatalytic processes. Besides, the intensity of the characteristic peak located at about $2\theta = 38.1°$ enhances, which is attributed to the (200) plane of cubic phase silver oxide and (111) plane of cubic phase silver (JCPDS No. 87-0597) (Zou et al. 2017). Moreover, three obvious characteristic peaks located at $2\theta = 44.3°$, 64.4° and 77.4° that are assigned to the (200), (220) and (311) planes of cubic phase silver are detected (Li and Huang 2015). These results demonstrate that the metallic Ag is formed by reducing of Ag_2O species through trapping the electrons generated from TiO_2 under UV light irradiation, which has been reported before (Cui et al. 2017).

Photocatalytic mechanism of the hierarchical Ag_2O-NP/TiO_2-NT nanocomposites

In order to determine the active species that exist in the processes of the photocatalytic degradation, p-BQ, EDTA-2Na, and IPA were employed as the scavengers for hydroxyl radicals ($^{\cdot}OH$), reactive holes (h^+), and superoxide radicals ($^{\cdot}O_2^-$) species, respectively. As shown in Fig. 9a, b, the $^{\cdot}OH$ species plays a dominant role in the photocatalytic degradation processes of the pure TiO_2 nanotubes photocatalyst, while the h^+ and $^{\cdot}O_2^-$ species for the 51.8%—Ag_2O-NP/TiO_2-NT photocatalyst (Zang et al. 2015; Huang et al. 2015). The corresponding pseudo-first-order simulation results of the degradation reactions are consistent with that as shown in Fig. S7 and Table S7, indicating the same results (Supplementary material).

It is well-known that the band edge positions of semiconductors play a significant impact on the photocatalytic processes, so they are calculated by the following equations (Wei et al. 2016):

$$E_{VB} = \chi - E^e + 0.5E_g \quad (5)$$

$$E_{CB} = E_{VB} - E_g \quad (6)$$

wherein, E_{VB}, E_{CB} and E_g are the valence band edge potential, conduction band edge potential, and the band gap estimated from the UV/Vis DRS experiments, respectively; χ is the geometric mean of the absolute electro negativity of all atoms in the semiconductor, and the values of titania and silver oxide are 5.81 and 5.29 eV (Kaur et al. 2017), respectively; E^e (ca. 4.5 eV) is the energy of free electrons on the hydrogen scale. Thus the E_{VB} and E_{CB} of titania were calculated to be 2.83 and − 0.21 eV, and the E_{VB} and E_{CB} of silver oxide were counted to be 1.88 and 0.42 eV, respectively.

On the basis of the above results, related possible photocatalytic mechanisms are speculated. When the pure TiO_2 nanotubes are employed as the photocatalyst (Fig. 9c), due to the more negative CB potential and higher VB potential of titania, the remaining

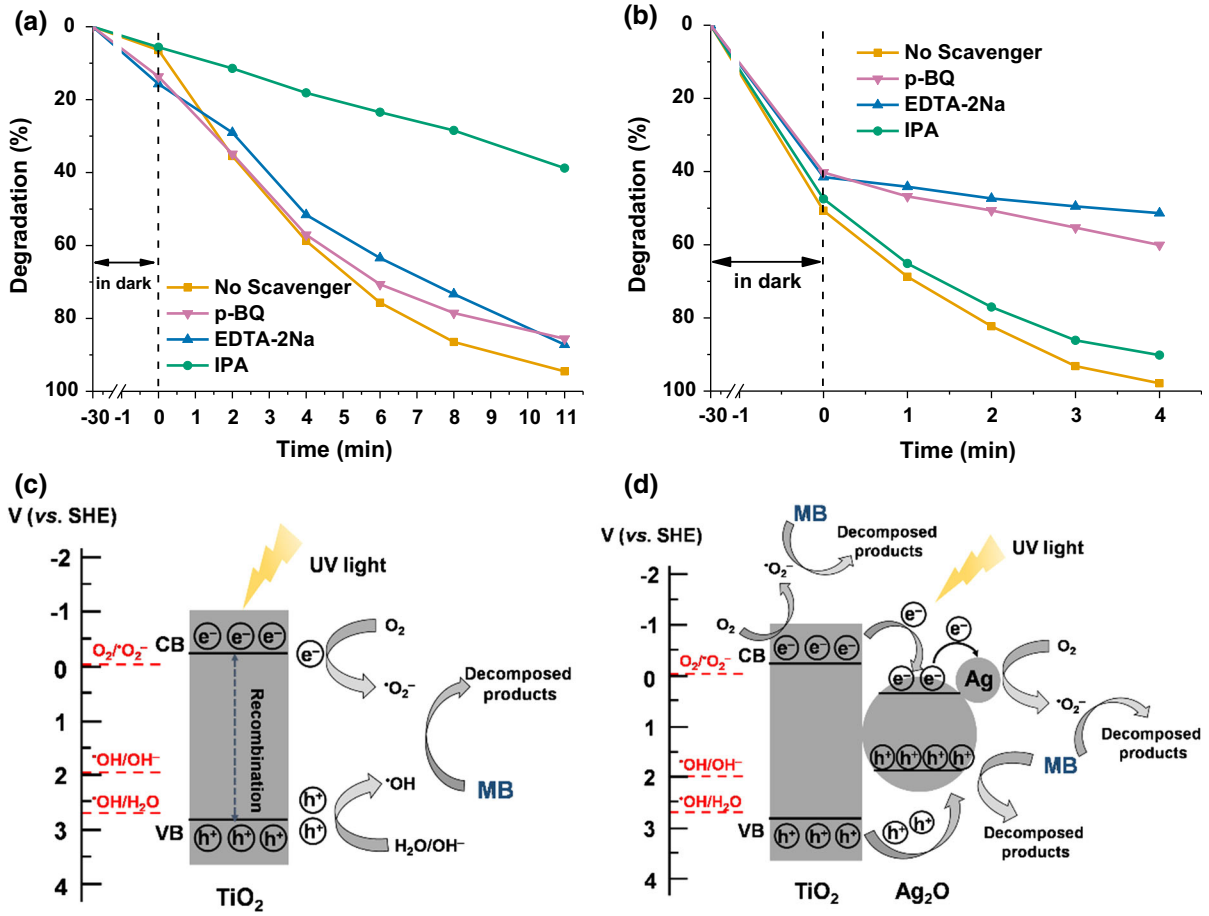

Fig. 9 The photocatalytic degradation profiles with the addition of scavengers of p-BQ, EDTA-2Na, and IPA in degrading MB and the purposed photocatalytic mechanisms of **a**, **c** the pure TiO_2 nanotubes, and **b**, **d** the cellulose-derived hierarchical 51.8%—Ag_2O-NP/TiO_2-NT nanocomposite under UV light irradiation

electrons after a rather fast recombination of the photogenerated electron–hole (e^-–h^+) pairs on the CB react with O_2 to generate $^{\cdot}O_2^-$, and holes on the VB react with H_2O or OH^- to generate $^{\cdot}OH$, and then the MB molecules are oxidized. Moreover, the $^{\cdot}OH$ species have a more important effect in oxidizing MB molecules than the $^{\cdot}O_2^-$ species, and the recombination of e^-–h^+ pairs is hindered when the holes are trapped, which is confirmed by the trapping experiments as discussed above.

Afterwards, as illustrated in Fig. 9d, when the Ag_2O nanoparticles are coated on the hierarchical TiO_2 nanotubes, and the Ag_2O-NP/TiO_2-NT heterostructure is formed at the interface, an inner electric filed ($TiO_2 \rightarrow Ag_2O$) is built. In view of the inner electric field and the energy band structure, the transfer of e^- from TiO_2 to Ag_2O is partially suppressed, while the transfer of h^+ is accelerated, leading to the efficient separation of e^-–h^+ pairs. Due to the lower VB potential and less negative CB potential of silver oxide, h^+ on the VB directly degrades MB molecules rather than react with H_2O or O_2 to produce $^{\cdot}OH$, and e^- on the CB is captured by metallic Ag, and then react with O_2 to produce $^{\cdot}O_2^-$ rather than directly react with O_2. Simultaneously, the plentiful remaining e^- on the CB of titania react directly with the trapped O_2 to generate $^{\cdot}O_2^-$, and a small number of h^+ on the VB react directly with H_2O or OH^- to generate $^{\cdot}OH$. Finally, the predominant reactive species h^+ and $^{\cdot}O_2^-$ together with trace amount of $^{\cdot}OH$ species degrade MB molecules, which is in accordance with the results of the trapping experiments.

Conclusions

In summary, a new bio-inspired hierarchical Ag_2O-NP/TiO_2-NT heterostructured nanocomposite is fabricated by the deposition of Ag_2O nanoparticles uniformly on the hierarchical anatase TiO_2 nanotubes that were templated by natural cellulose substance (commercial laboratory filter paper). When it is employed as the photocatalysts in degrading the organic pollutants, it exhibits improved activity by contrast with the pure TiO_2 nanotubes and Ag_2O nanoparticles. Furthermore, it also shows superior photocatalytic performance than other reported Ag_2O/TiO_2 composites due to the unique structures that derived from the initial cellulose substance. We have demonstrated the initial hypothesis that the hierarchical network porous structure and effective formation of the heterostructures between the titania and silver oxide phases possessed by the Ag_2O-NP/TiO_2-NT nanocomposites result in the enhanced photocatalytic performances, which is attributed to the unique structure and superior surface properties of the natural cellulose substance. We also reveal the relationship in-between the structures and photocatalytic activities of such a cellulose substance derived material. It provides a new sight on designing efficient photocatalytic materials for waste water treatment by combining the fascinating structures of the natural substance and the specific physicochemical properties of the guest species.

Acknowledgments This work was supported by the Zhejiang Provincial Natural Science Foundation of China (LY16B010001).

Compliance with ethical standards

Conflict of interest The authors declare no conflict of interest.

References

Aboamera NM, Mohamed A, Salama A, Osman TA, Khattab A (2018) An effective removal of organic dyes using surface functionalized cellulose acetate/graphene oxide composite nanofibers. Cellulose 25:4155–4166

Ariga K, Yamauchi Y, Mori T, Hill JP (2013) 25th anniversary article: what can be done with the Langmuir–Blodgett method? Recent developments and its critical role in materials science. Adv Mater 25:6477–6512

Ariga K, Yamauchi Y, Rydzek G, Ji Q, Yonamine Y, Wu KCW, Hill JP (2014) Layer-by-layer nanoarchitectonics: invention, innovation, and evolution. Chem Lett 43:36–68

Cai P, Feng X, Fei J, Li G, Li J, Huang J, Li J (2015) Co-assembly of photosystem II/reduced graphene oxide multilayered biohybrid films for enhanced photocurrent. Nanoscale 7:10908–10911

Chen W, Yu H, Lee SY, Wei T, Li J, Fan Z (2018) Nanocellulose: a promising nanomaterial for advanced electrochemical energy storage. Chem Soc Rev 47:2837–2872

Chu H, Liu X, Liu J, Li J, Wu T, Li H, Lei W, Xu Y, Pan L (2016) Synergetic effect of Ag_2O as co-catalyst for enhanced photocatalytic degradation of phenol on N-TiO_2. Mater Sci Eng B Adv 211:128–134

Cui Y, Ma Q, Deng X, Meng Q, Cheng X, Xie M, Li X, Cheng Q, Liu H (2017) Fabrication of Ag-Ag_2O/reduced TiO_2 nanophotocatalyst and its enhanced visible light driven photocatalytic performance for degradation of diclofenac solution. Appl Catal B Environ 206:136–145

Fei J, Li J (2015) Controlled preparation of porous TiO_2-Ag nanostructures through supramolecular assembly for plasmon-enhanced photocatalysis. Adv Mater 27:314–319

Fujishima A, Honda K (1972) Photolysis-decomposition of water at surface of an irradiated semiconductor. Nature 238:238–245

Gao R, Lu Y, Xiao S, Li J (2017) Facile fabrication of nanofibrillated chitin/Ag_2O heterostructured aerogels with high iodine capture efficiency. Sci Rep 7:4303–4311

Gu Y, Huang J (2013) Precise size control over ultrafine rutile titania nanocrystallites in hierarchical nanotubular silica/titania hybrids with efficient photocatalytic activity. Chem Eur J 19:10971–10981

Hao C, Wang W, Zhang R, Zou B, Shi H (2018) Enhanced photoelectrochemical water splitting with TiO_2@Ag_2O nanowire arrays via p-n heterojunction formation. Sol Energy Mater Sol Cells 174:132–139

Hu X, Liu X, Tian J, Li Y, Cui H (2017) Towards full-spectrum (UV, visible, and near-infrared) photocatalysis: achieving an all-solid-state Z-scheme between Ag_2O and TiO_2 using reduced graphene oxide as the electron mediator. Catal Sci Technol 7:4193–4205

Huang Z, Sun Q, Lv K, Zhang Z, Li M, Li B (2015) Effect of contact interface between TiO_2 and g-C_3N_4 on the photoreactivity of g-C_3N4/TiO_2 photocatalyst: (001) vs (101) facets of TiO_2. Appl Catal B Environ 164:420–427

Ishimaki K, Uchiyama T, Okazaki M, Lu D, Uchimoto Y, Maeda K (2018) Influence of TiO_2 support on activity of Co_3O_4/TiO_2 photocatalysts for visible-light water oxidation. Bull Chem Soc Jpn 91:486–491

Jia Y, Li J (2015) Molecular assembly of Schiff base interactions: construction and application. Chem Rev 115:1597–1621

Jiang W, Wang X, Wu Z, Yue X, Yuan S, Lu H, Liang B (2015) Silver oxide as superb and stable photocatalyst under visible and near-infrared light irradiation and its photocatalytic mechanism. Ind Eng Chem Res 54:832–841

Kansal SK, Singh M, Sud D (2008) Studies on TiO_2/ZnO photocatalysed degradation of lignin. J Hazard Mater 153:412–417

Kaur A, Salunke DB, Umar A, Mehta SK, Sinha ASK, Kansal SK (2017) Visible light driven photocatalytic degradation of fluoroquinolone levofloxacin drug using Ag_2O/TiO_2 quantum dots: a mechanistic study and degradation pathway. New J Chem 41:12079–12090

Kim ML, Otal EH, Hinestroza JP (2019) Cellulose meets reticular chemistry: interactions between cellulosic substrates and metal–organic frameworks. Cellulose 26:123–137

Kumar D, Reddy N, Karthik M, Neppolian B, Madhavan J, Shankar M (2016) Solar light sensitized p-Ag_2O/n-TiO_2 nanotubes heterojunction photocatalysts for enhanced hydrogen production in aqueous-glycerol solution. Sol Energy Mater Sol Cells 154:78–87

Lalitha K, Reddy JK, Sharma MVP, Kumari VD, Subrahmanyam M (2010) Continuous hydrogen production activity over finely dispersed Ag_2O/TiO_2 catalysts from methanol: water mixtures under solar irradiation: a structure-activity correlation. Int J Hydrogen Energy 35:3991–4001

Li S, Huang J (2015) A nanofibrous silver-nanoparticle/titania/carbon composite as anode material for lithium ion batteries. J Mater Chem A 3:4354–4360

Li S, Huang J (2016) Cellulose-rich nanofiber-based functional nanoarchitectures. Adv Mater 28:1143–1158

Li G, Zhang D, Yu J (2009) A new visible-light photocatalyst: CdS quantum dots embedded mesoporous TiO_2. Environ Sci Technol 43:7079–7085

Li J, Feng X, Fei J, Cai P, Huang J, Li J (2016) Integrating photosystem II into a porous TiO_2 nanotube network toward highly efficient photo-bioelectrochemical cells. J Mater Chem A 4:12197–12204

Li G, Fei J, Xu Y, Li Y, Li J (2018a) Bioinspired assembly of hierarchical light-harvesting architectures for improved photophosphorylation. Adv Funct Mater 28:1706557

Li S, Qi D, Huang J (2018b) Natural cellulose based self-assembly towards designed functionalities. Curr Opin Colloid Interface Sci 35:1–8

Linsebigler AL, Lu GQ, Yates YT (1995) Photocatalysis on TiO_2 surfaces: principles, mechanisms, and selected results. Chem Rev 95:735–758

Liu X, Gu Y, Huang J (2010) Hierarchical titania-coated, carbon nanofibrous material derived from a natural cellulose substance. Chem Eur J 16:7730–7740

Liu C, Cao C, Luo X, Luo S (2015a) Ag-bridged Ag_2O nanowire network/TiO_2 nanotube array p-n heterojunction as a highly efficient and stable visible light photocatalyst. J Hazard Mater 285:319–324

Liu X, Li J, Zhang Y, Huang J (2015b) Bio-inspired hierarchical nanotubular titania immobilized with platinum nanoparticles for photocatalytic hydrogen production. Chem Eur J 21:7345–7349

Liu B, Mu L, Han B, Zhang J, Shi H (2017) Fabrication of TiO_2/Ag_2O heterostructure with enhanced photocatalytic and antibacterial activities under visible light irradiation. Appl Surf Sci 396:1596–1603

Liu G, Wang G, Hu Z, Su Y, Zhao L (2019) Ag_2O nanoparticles decorated TiO_2 nanofibers as a p-n heterojunction for enhanced photocatalytic decomposition of RhB under visible light irradiation. Appl Surf Sci 465:902–910

Luo Y, Huang J (2015) Hierarchical structured anatase-titania/cellulose composite sheet with high photocatalytic performance and antibacterial activity. Chem Eur J 21:2568–2575

Luo Y, Xu J, Huang J (2014) Hierarchical nanofibrous anatase-titania/cellulose composite and its photocatalytic property. CrystEngComm 16:464–471

Mandari KK, Kwak BS, Police AKR, Kang M (2017) In-situ photo-reduction of silver particles and their SPR effect in enhancing the photocatalytic water splitting of Ag_2O/TiO_2 photocatalysts under solar light irradiation: a case study. Mater Res Bull 95:515–524

Min KS, Kumar RS, Lee JH, Kim KS, Lee SG, Son YA (2019) Synthesis of new TiO_2/porphyrin-based composites and photocatalytic studies on methylene blue degradation. Dyes Pigment 160:37–47

Mohamed MA, Salleh WNW, Jaafar J, Rosmi MS, Hir ZAM, Mutalib MA, Ismail AF, Tanemura M (2017) Carbon as amorphous shell and interstitial dopant in mesoporous rutile TiO_2: bio-template assisted sol-gel synthesis and photocatalytic activity. Appl Surf Sci 393:46–59

Mohamed MA, Zain MFM, Minggu LJ, Kassim MB, Amid NAS, Salleh WNW, Salehmin MNI, Nasir MFM, Hir ZAM (2018) Constructing bio-templated 3D porous microtubular C-doped g-C_3N_4 with tunable band structure and enhanced charge carrier separation. Appl Catal B Environ 236:265–279

Paul MM, Ghosh R, Giri PK (2016) Mechanism of strong visible light photocatalysis by Ag_2O-nanoparticle-decorated monoclinic TiO_2(B) porous nanorods. Nanotechnology 27:315703

Sarkar D, Ghosh C, Mukherjee S, Chattopadhyay K (2013) Three dimensional Ag_2O/TiO_2 type-II (p-n) nanoheterojunctions for superior photocatalytic activity. ACS Appl Mater Interfaces 5:331–337

Su X, Liao Q, Liu L, Meng R, Qian Z, Gao H, Yao J (2017) Cu_2O nanoparticle-functionalized cellulose-based aerogel as high-performance visible-light photocatalyst. Cellulose 24:1017–1029

Wang H, Wang C, Cui X, Qin L, Ding R, Wang L, Liu Z, Zheng Z, Lv B (2018a) Design and facile one-step synthesis of $FeWO_4/Fe_2O_3$ di-modified WO_3 with super high photocatalytic activity toward degradation of quasi-phenothiazine dye. Appl Catal B Environ 221:169–178

Wang JC, Lou HH, Xu ZH, Cui CX, Li ZJ, Jiang K, Zhang YP, Qu LB, Shi W (2018b) Natural sunlight driven highly efficient photocatalysis for simultaneous degradation of rhodamine B and methyl orange using I/C codoped TiO_2 photocatalyst. J Hazard Mater 360:356–363

Wei W, Mao X, Ortiz LA, Sadoway DR (2011) Oriented silver oxide nanostructures synthesized through a template-free electrochemical route. J Mater Chem 21:432–438

Wei N, Cui H, Song Q, Zhang L, Song X, Wang K, Zhang Y, Li J, Wen J, Tian J (2016) Ag_2O nanoparticle/TiO_2 nanobelt heterostructure with remarkable photo-response and photocatalytic properties under UV, visible and near-infrared irradiation. Appl Catal B Environ 198:83–90

Xiao H, Zhang W, Wei Y, Chen L (2018) Carbon/ZnO nanorods composites templated by TEMPO oxidized cellulose and

photocatalytic activity for dye degradation. Cellulose 25:1809–1819

Xu F, Zhang J, Zhu B, Yu J, Xu J (2018) $CuInS_2$ sensitized TiO_2 hybrid nanofibers for improved photocatalytic CO_2 reduction. Appl Catal B Environ 230:194–202

Yoon YH, Lee SY, Gwon JG, Cho HJ, Wu Q, Kim YH, Lee WH (2018) Photocatalytic performance of highly transparent and mesoporous molybdenum-doped titania films fabricated by templating cellulose nanocrystals. Ceram Int 44:16647–16653

Yu W, Liu X, Chu H, Zhu G, Li J, Liu J, Niu L, Sun Z, Pan L (2015) Enhancement of visible light photocatalytic activity of Ag_2O/F-TiO_2 composite. J Mol Catal A Chem 407:25–31

Zakaria MB, Li C, Ji Q, Jiang B, Tominaka S, Ide Y, Hill JP, Ariga K, Yamauchi Y (2016) Self-construction from 2D to 3D: one-pot layer-by-layer assembly of graphene oxide sheets held together by coordination polymers. Angew Chem Int Ed 55:8426–8430

Zang M, Shi L, Liang L, Li D, Sun J (2015) Heterostructured g-C_3N_4/Ag–TiO_2 composites with efficient photocatalytic performance under visible-light irradiation. RSC Adv 5:56136–56144

Zelekew OA, Kuo DH, Yassin JM, Ahmed KE, Abdullah H (2017) Synthesis of efficient silica supported TiO_2/Ag_2O heterostructured catalyst with enhanced photocatalytic performance. Appl Surf Sci 410:454–463

Zhou W, Liu H, Wang J, Liu D, Du G, Cui J (2010) Ag_2O/TiO_2 nanobelts heterostructure with enhanced ultraviolet and visible photocatalytic activity. ACS Appl Mater Interfaces 2:2385–2392

Zou M, Liu H, Feng L, Xiong F, Thomas T, Yang M (2017) Effect of nitridation on visible light photocatalytic behavior of microporous (Ag, Ag_2O) co-loaded TiO_2. Microporous Mesoporous Mater 240:137–144